ARTICLE

Tks5 and Dynamin-2 enhance actin bundle rigidity in invadosomes to promote myoblast fusion

Mei-Chun Chuang[1], Shan-Shan Lin[1], Ryosuke L. Ohniwa[2,3], Gang-Hui Lee[4] , You-An Su[1], Yu-Chen Chang[1], Ming-Jer Tang[4,5], and Ya-Wen Liu[1,6]

Skeletal muscle development requires the cell–cell fusion of differentiated myoblasts to form muscle fibers. The actin cytoskeleton is known to be the main driving force for myoblast fusion; however, how actin is organized to direct intercellular fusion remains unclear. Here we show that an actin- and dynamin-2–enriched protrusive structure, the invadosome, is required for the fusion process of myogenesis. Upon differentiation, myoblasts acquire the ability to form invadosomes through isoform switching of a critical invadosome scaffold protein, Tks5. Tks5 directly interacts with and recruits dynamin-2 to the invadosome and regulates its assembly around actin filaments to strengthen the stiffness of dynamin-actin bundles and invadosomes. These findings provide a mechanistic framework for the acquisition of myogenic fusion machinery during myogenesis and reveal a novel structural function for Tks5 and dynamin-2 in organizing actin filaments in the invadosome to drive membrane fusion.

Introduction

Cell–cell fusion is essential for the development and homeostasis of multicellular organisms (Chen et al., 2007; Oren-Suissa and Podbilewicz, 2007). Eukaryotic cells must use unique protein machineries to overcome the energy barrier required for fusion of two lipid bilayers (Kozlovsky and Kozlov, 2002; Chen and Olson, 2005; Kozlov and Chernomordik, 2015). The best-studied membrane fusion event is that between synaptic vesicles and the plasma membrane, which requires tethering factors, SNAREs, synaptotagmins, and Rabs to orchestrate the recognition and merging of two membranes (McMahon et al., 2010; Jahn and Fasshauer, 2012). In contrast, the molecular mechanisms driving the topologically opposite membrane fusion between two cells are less understood.

Among the cell–cell fusion processes that occur in different tissues or organisms, myoblast fusion in *Drosophila melanogaster* is one of the most well characterized (Abmayr and Pavlath, 2012; Kim et al., 2015a; Rodal et al., 2015). These studies have established the actin cytoskeleton as the driving force for myoblast fusion (Srinivas et al., 2007; Vasyutina et al., 2009; Sens et al., 2010; Shilagardi et al., 2013). In the fly embryo, actin is asymmetrically organized between two fusing myoblasts: the fusion competent myoblast protrudes a WASP and Arp2/3-mediated actin protrusion, whereas the founder cell mounts a resistant force from cortical actin (Sens et al., 2010; Kim et al., 2015a). In

combination, the mechanical tension built up by the protrusive and resisting forces propels the myoblast membranes into close enough apposition to fuse (Kozlov and Chernomordik, 2015; Duan et al., 2018). However, how myoblasts obtain the ability to form protrusive actin structures and how actin is organized to meet this unique cellular demand remain unclear.

Recently, the membrane remodeling GTPase, dynamin-2 (Dyn2), was reported to be involved in myoblast and osteoclast fusion, although its exact role remains unknown (Leikina et al., 2013; Shin et al., 2014). Dyn2 is a ubiquitously expressed mechanochemical enzyme best studied for its role in catalyzing membrane fission during endocytosis. However, it has also been shown to reorganize the actin cytoskeleton in structures such as lamellipodia and podosomes (Schmid and Frolov, 2011; Ferguson and De Camilli, 2012; Sever et al., 2013; Antonny et al., 2016). Which of these activities are required for membrane fusion has not been established.

Podosomes are membrane-bound, actin-enriched invasive structures that are abundant in monocytic cells and responsible for cell adhesion, migration, mechanosensing, extracellular matrix degradation, and invasion (Albiges-Rizo et al., 2009; Schachtner et al., 2013; Linder and Wiesner, 2015). Similar structures, called invadopodia, can be found in cancer cells and are important for invasion and metastasis (Murphy and

[1]Institute of Molecular Medicine, College of Medicine, National Taiwan University, Taipei, Taiwan; [2]Faculty of Medicine, University of Tsukuba, Tsukuba, Japan; [3]Center for Biotechnology, National Taiwan University, Taipei, Taiwan; [4]International Center of Wound Repair and Regeneration, National Cheng Kung University, Tainan, Taiwan; [5]Department of Physiology, Medical College, National Cheng Kung University, Tainan, Taiwan; [6]Center of Precision Medicine, College of Medicine, National Taiwan University, Taipei, Taiwan.

Correspondence to Ya-Wen Liu: yawenliu@ntu.edu.tw.

Courtneidge, 2011). Therefore, podosomes and invadopodia, together named "invadosomes," are best known for their invasion abilities in both normal and cancer cells.

The formation of invadosomes is tightly controlled by chemical signaling pathways, such as integrin- and/or growth factor receptor–stimulated phosphoinositide 3-kinase and Src kinase activities, as well as by their physical microenvironment, e.g., matrix stiffness and traction force (Labernadie et al., 2010; Murphy and Courtneidge, 2011; Yu et al., 2013). One of the critical regulators of invadosome function is tyrosine kinase substrate with 5 SH3 domain (Tks5), which is activated by Src and localizes to the plasma membrane through binding with phosphatidylinositol(3,4)bisphosphate (Seals et al., 2005; Sharma et al., 2012). Activated Tks5 recruits actin polymerization regulators, such as N-WASP, Nck, and Grb2, to the membrane, hence promoting the maturation and function of invadosomes (Oikawa et al., 2008; Sharma et al., 2013; Saini and Courtneidge, 2018). Importantly, Tks5 has been reported to be critical for osteoclast fusion (Oikawa et al., 2012). Therefore, we hypothesize that invadosome and Dyn2 may be directly involved in myoblast fusion during myogenesis. Here we report that Tks5-mediated invadosome formation is required for mammalian myoblast fusion and show that Tks5 regulates Dyn2 assembly around actin bundles, strengthening them to propel membrane fusion.

Results

Invadosomes form in differentiated myoblasts before fusion
We used murine myoblast C2C12 cells, which recapitulate myogenic differentiation and fusion when incubated with differentiation medium (DM), to monitor myoblast fusion (Blau et al., 1985). After 3 d in DM, myoblasts became spindle-shaped and started to fuse, leading to their maturation into multinuclear myotubes within another 2 d (Fig. S1 A).

We first examined the expression and distribution of invadosome components Tks5, Dyn2, and Cortactin during myogenesis. The protein levels of Tks5 and Dyn2 gradually increased upon myoblast differentiation and reached approximately threefold after 5 d of differentiation, whereas Cortactin, which is enriched in invadosomes but also associated with other actin structures, was less up-regulated (Fig. 1 A). To have proper cell density for imaging, differentiated myoblasts (∼56 h in DM) were trypsinized and subcultured onto fibronectin-coated coverslips for 16 h before immunofluorescence staining. Under these conditions, we found that differentiated myoblasts are often equipped with F-actin foci at their tips, together with many well-known invadosome proteins, including MT1-MMP, Tks5, Dyn2, Cortactin, and Arp2/3, even when not in contact with other myoblasts (Fig. 1, B and C; and Fig. S1, B and C). This distribution of Dyn2 and Tks5 was distinct from their localization in undifferentiated myoblasts that were mainly at clathrin-coated pits (CCPs) or cytosol, respectively (Fig. S1, D and E).

To further characterize the actin-Dyn2 enriched structure we observed in mouse myoblasts, we examined the ECM degradation ability of differentiated myoblasts (Fig. 1 D). Although we

did not detect ECM degradation in the invadosome formed at the myoblast tip, evident ECM degradation was observed when invadosomes were formed at the central area of the cell (Fig. 1 D). Thus the tips of prefusion mouse myoblasts bear the molecular signature of an invadosome, which was similar to the WASP-Arp2/3 complex–mediated protrusive structure that propels myoblast fusion in *Drosophila* (Sens et al., 2010).

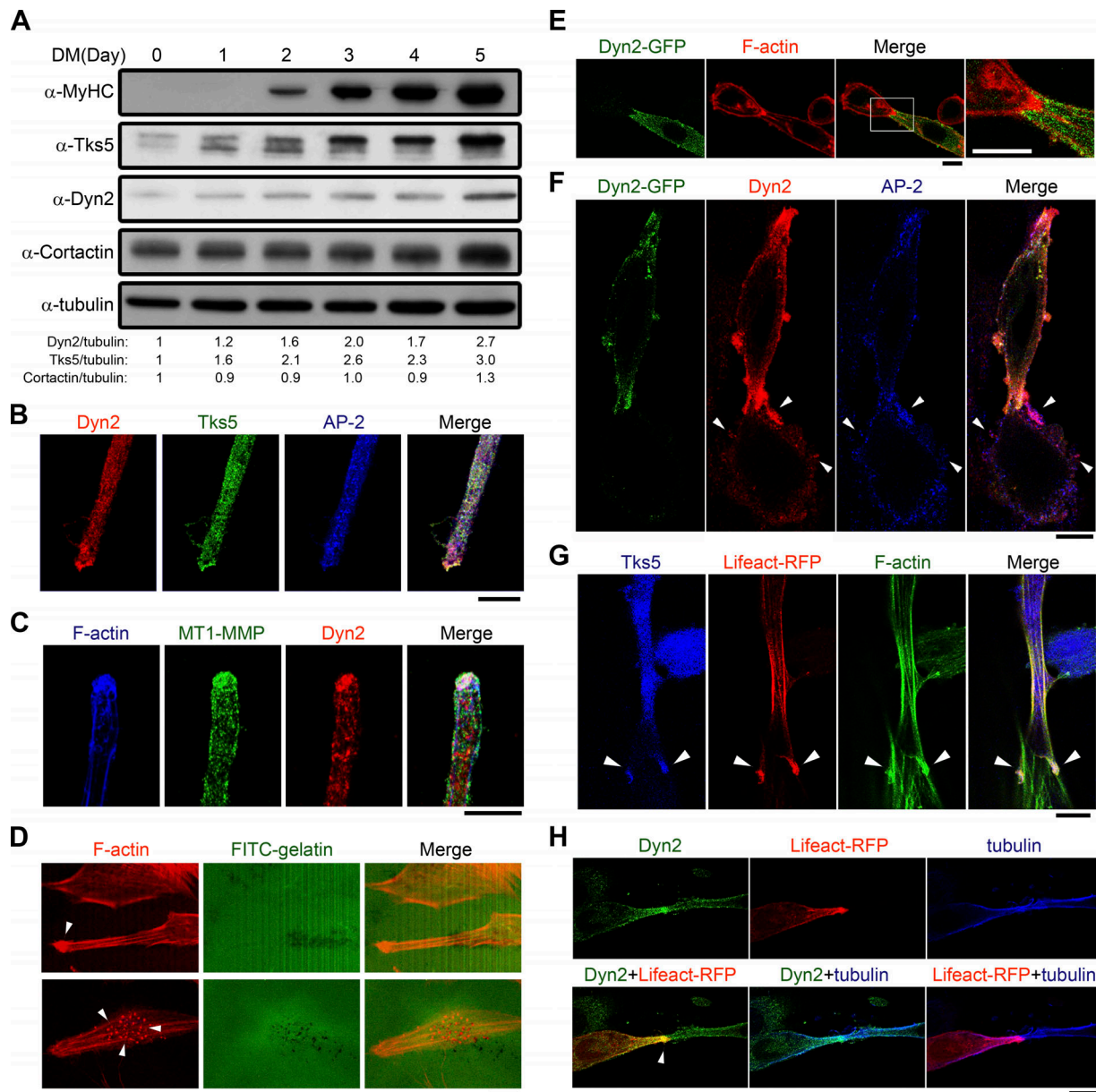### Asymmetrical distribution of invadosome in fusing myoblasts
To determine whether the invadosome is equipped in two fusing myoblasts, we imaged cells near confluence with one cell expressing Dyn2-GFP to label the cell boundary. Under these conditions, staining of F-actin revealed that only one of the paired cells exhibited an actin-based protrusive structure, while the F-actin in the opposing cell distributed evenly throughout the cell surface (Fig. 1 E). The asymmetrical enrichment could also be observed with Dyn2 and Tks5, where one myoblast exhibits a Dyn2-GFP– or Tks5-rich protrusion to "attack" the opposing myoblast, which instead has mainly Dyn2 colocalized with the CCPs, labeled by clathrin adaptor AP-2, or cytosolic Tks5 (Fig. 1, F and G). Importantly, in the receiving cell, Dyn2 was not concentrated at the fusion interface (Fig. 1 E).

To further verify the asymmetric distribution of the invadosome in two fusing myoblasts, we analyzed the distribution of endogenous Dyn2 in myoblasts labeled with the F-actin marker Lifeact-RFP (Fig. 1 H). Consistent with the data above, the enrichment of endogenous Dyn2 at the tip was observed only in the attacking cell together with the F-actin focus (Fig. 1 H, arrowhead). Of note, tubulin localized equally in both myoblasts, indicating that the asymmetrical distribution is not a general feature for all cytoskeletal proteins. Altogether, in these data we observed asymmetrical formation of an invadosome in differentiated myoblasts.

Invadosome-equipped tips are sites of intercellular fusion
The formation of invadosome at the tip of differentiated myoblasts was reminiscent of the actin focus found in *Drosophila* myoblasts where intercellular fusion takes place (Sens et al., 2010). To examine whether the Dyn2/actin-enriched myoblast tip is where cell–cell fusion occurs, we used GFP-tagged Dyn2 to monitor its localization in real time. We first confirmed that exogenous Dyn2-GFP, similar to endogenous Dyn2, colocalizes with mCherry-actin at the tip of the differentiated myoblast, and they form protrusive structures when this myoblast is tightly juxtaposed with another myoblast (Fig. 2 A). With time-lapse microscopy, we found that Dyn2-GFP enriches at the tip of a differentiated mononuclear myoblast and protrudes toward its neighboring cell, another mononuclear myoblast, at time 0 and 5 min in Fig. 2 B. At 10 min, the finger-like structure disappeared, and diffuse Dyn2-GFP labeling could be detected in the neighboring myoblast, indicative of fusion. By 20 min, the cytoplasm was completely mixed (Fig. 2 B and Video 1). It is worth noting that the number of successful fusion events is low in myoblasts under fluorescent microscopy, thus resulting in a low efficiency to capture invadosome formation during fusion.

In addition to the fusion between two mononuclear myoblasts, the so-called first-phase fusion, we also observed

Chuang et al.
Dynamin-2 promotes myoblast fusion via actin bundling ability

Journal of Cell Biology 1671
https://doi.org/10.1083/jcb.201809161

Figure 1. **Invadosome forms and distributes asymmetrically in differentiated myoblasts. (A)** Expression level of different invadosome components in myoblasts upon differentiation. Myoblast lysates derived from different days of DM treatment were immunoblotted with indicated antibodies. Numbers below indicate the fold-change of Dyn2, Tks5, and Cortactin compared with day 0 after normalization with tubulin. **(B and C)** Colocalization of invadosome components at the myoblast tip of differentiated myoblast. Day 3 differentiated C2C12 myoblasts were immunofluorescence stained to detect endogenous Tks5, Dyn2, MT1-MMP, F-actin, and AP-2. Images were acquired with z-stack confocal microscopy and shown as single focal planes. **(D)** Matrix degradation ability. Day 3 differentiated myoblasts were seeded onto an FITC–gelatin–coated coverslip and imaged after 24 h. Arrowheads indicate invadosomes. **(E–H)** Asymmetrical distribution of invadosome in fusing myoblasts. Two close-positioned, day 3 differentiated myoblasts with one cell labeled with Dyn2-GFP or Lifeact-RFP were stained for F-actin (E), Dyn2 and AP-2 (F), Tks5 (G), and tubulin (H). Arrowheads in F indicate the enriched Dyn2 and AP2 at the cell periphery of the receiving cell or the invadosome in attacking cells (G and H). Scale bars (both black and white), 10 μm.

Dyn2-GFP enrichment during the fusion between a nascent myotube and an additional myoblast or myotube, also known as second-phase fusion (Fig. 2 C). As in first-phase fusion, Dyn2-GFP was enriched at the interface between two fusing myotubes, and they formed foci right before fusion occurred (arrowheads in Fig. 2 C). At time 20 min, Dyn2-GFP diffused slowly throughout the large myotube, yet the loss of fluorescence in the attacking cell is readily observable. However, in this case the actin- and

Dyn2-enriched foci were localized between adjacent cells and not at obvious cell tips. Nonetheless, the protrusive characteristic of Dyn2 foci could be clearly illustrated with a failed attempt to fuse (Fig. S1 F). At time 0, Dyn2-GFP was enriched at the plasma membrane between two myoblasts, and a cone-shaped Dyn2-GFP focus gradually formed and protruded toward its neighboring myotube labeled with Dyn2-mCherry (Fig. S1 F, 5–25 min). Similar protrusions could also be observed when cells were
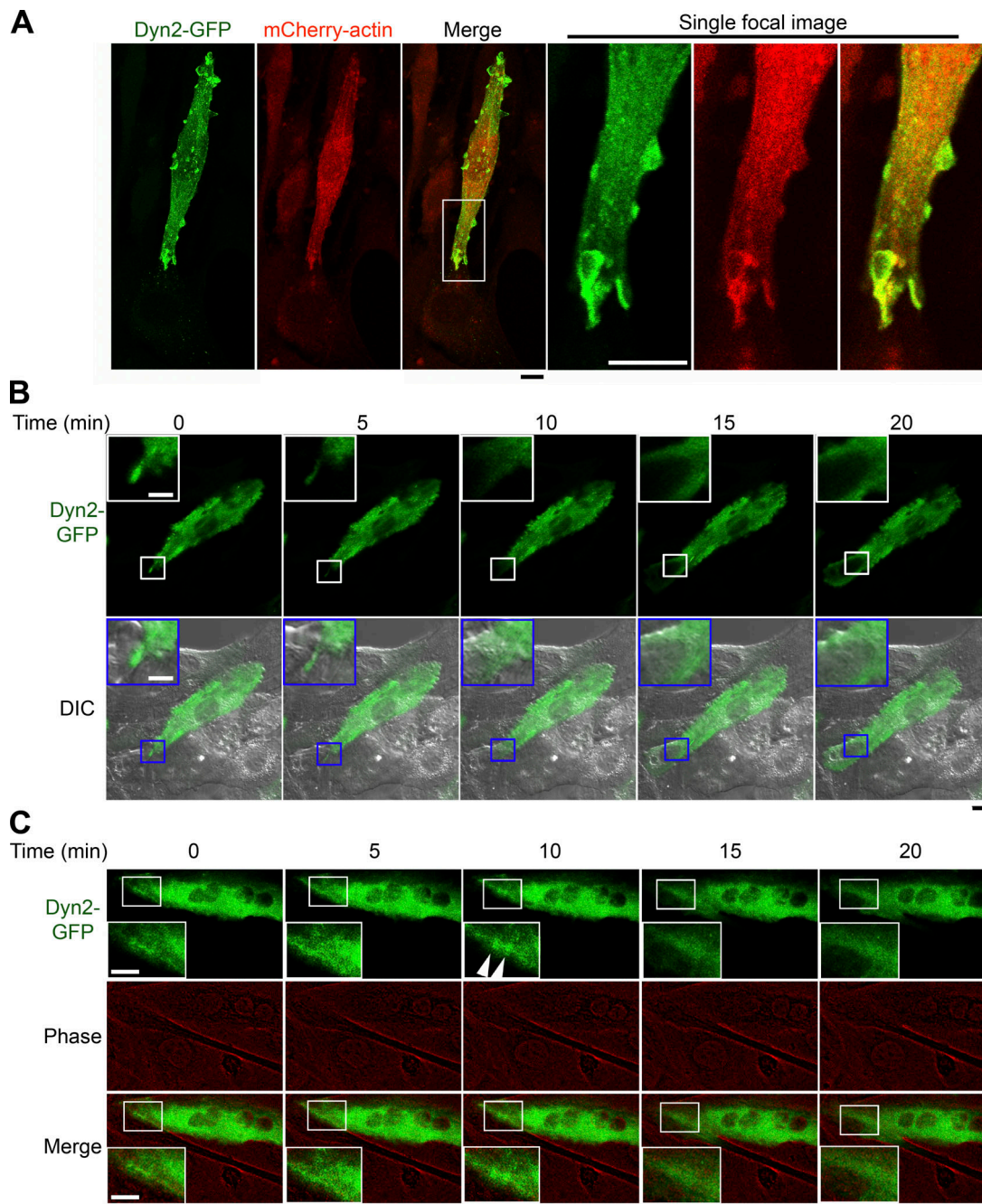
Figure 2. **Dyn2 enriches at myoblast fusion site. (A)** Dyn2-GFP and actin-based finger-like structures in differentiated myoblasts. Differentiated C2C12-expressing Dyn2-GFP and mCherry-actin was fixed and imaged with z-stack confocal microscopy. Maximum-intensity projections are shown, while magnified insets are single focal images. Scale bars (black and white), 10 µm. **(B)** Dyn2-GFP enrichment at the site of myoblast fusion. The dynamic localization of Dyn2-GFP in day 3 differentiated C2C12 was monitored with time-lapse microscopy. Five frames right before and after myoblast fusion from a 5-h recording were extracted and shown. Boxed regions were enlarged and shown in insets. Scale bars (black and white), 10 µm. **(C)** Dyn2-rich membrane protrusion in second-phase myoblast fusion. Time-lapse microscopic imaging of Dyn2-GFP in day 4 differentiated C2C12. Phase-contrast image was pseudocolored to better observe the boundary between two myotubes. White arrowheads indicate the Dyn2-GFP foci at the fusion interface. Black bar, 20 µm. White bar, 10 µm.

labeled with Lifeact-RFP, indicating that these protrusive structures are not artifacts resulting from Dyn2-GFP overexpression (Fig. S1 G). Together, these results demonstrate the transient formation of invadosomes at the interface of fusing myoblasts 5–10 min before fusion.

The invadosome is indispensable for myoblast fusion

Tks5 is an invadosome scaffold protein that is critical for invadosome maturation and function (Seals et al., 2005). To explore the contribution of invadosomes to myoblast fusion, we performed shRNA knockdown experiments. Silencing Tks5 with shRNA did
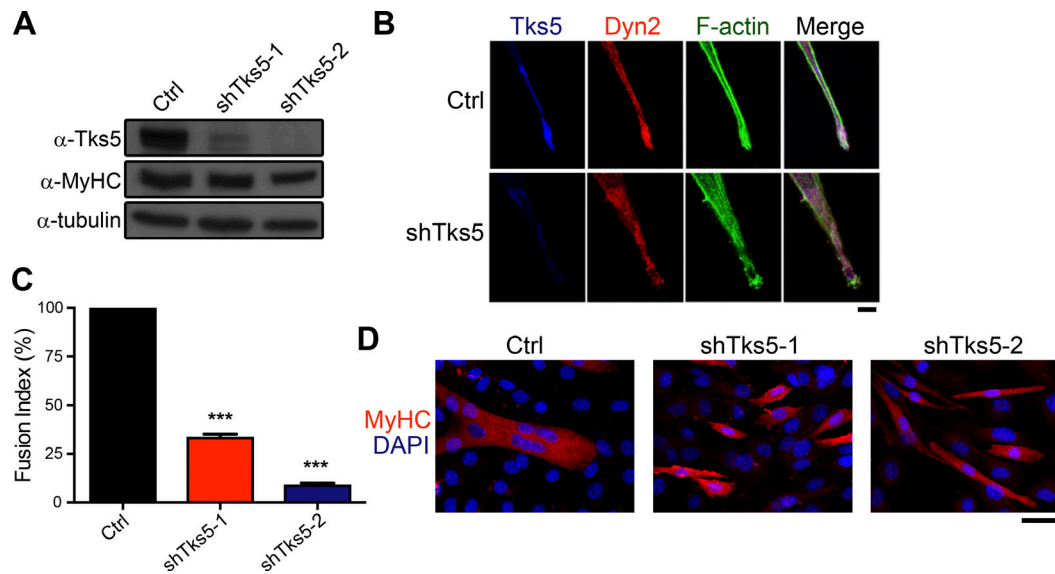
Figure 3. **Invadosome is required for myoblast fusion. (A and B)** Differentiation and morphology of Tks5-depleted myoblasts. Tks5 was depleted by two lentiviral shRNAs and selected with puromycin for 3 d. After 3 d of DM treatment, cells were processed for immunoblotting (A) or immunostaining (B). Scale bar, 10 μm. **(C and D)** Myoblast fusion in Tks5-depleted myoblasts. Fusion efficiency was analyzed in day 4 DM-treated myoblasts by immunofluorescent staining and quantified as number of nuclei in multinuclear cell (nuclear number ≥3)/number of nuclei in MyHC-positive cell. Fusion efficiency is considered as 100% in control cells. Scale bar, 50 μm. All values reported in this study represent the mean ± SD of at least three independent experiments, and data were analyzed with one-way ANOVA. ***, $P < 0.001$.

not perturb myoblast differentiation, as comparable amounts of myosin heavy chain (MyHC) were detected (Fig. 3 A). Moreover, Tks5-depleted myoblasts could differentiate into spindle-shaped myoblasts, yet there was no Dyn2/actin-enriched invadosome at the tip (Fig. 3 B). Importantly, the fusion efficiency, quantified by the percentage of differentiated myoblasts with more than three nuclei, was significantly impaired in Tks5 knockdown cells (Fig. 3, C and D). These results demonstrate that the invadosome is required for myoblast fusion, but not differentiation.

Isoform switching of Tks5 upon myoblast differentiation
Interestingly, immunoblotting with anti-Tks5 SH3 domain antibody showed multiple bands with molecular weights ranging from 130 to 150 kD in undifferentiated myoblasts, whereas only the 150-kD band increased upon DM treatment (Fig. 1 A). It is known that alternative transcription of Tks5 can result in two shorter isoforms, Tks5$_{short}$ and Tks5β, which lack the N-terminal membrane binding PX domain (Fig. 4 A; Li et al., 2013; Cejudo-Martin et al., 2014). Thus, these shorter isoforms are expected to function as dominant negative forms perturbing the activity of long form of Tks5 (Tks5α; Saini and Courtneidge, 2018). To test whether Tks5 undergoes isoform switching during myogenesis, we examined Tks5 with antibodies recognizing the SH3 and PX domains. The anti-Tks5 SH3 antibody detected all Tks5 isoforms in both undifferentiated and differentiated lysates, whereas anti-Tks5 PX domain antibody recognized only Tks5α at 150 kD (Fig. 4 B). Furthermore, the protein expression level of Tks5α, but not Tks5$_{short}$ and Tks5β, significantly increased upon differentiation (Fig. 4 C).

To further confirm the switch of Tks5 isoforms, we used primers that distinguish Tks5β from Tsk5α (Cejudo-Martin

et al., 2014; exon 6β and PX domain, respectively) and performed quantitative PCR to measure Tks5α and Tks5β mRNA levels in differentiated and undifferentiated myoblasts (Fig. 4 D). Similar to our immunoblotting result, the mRNA level of Tks5α, but not Tks5β, increased significantly upon myoblast differentiation. This isoform switch results in an increased protein ratio of Tks5α/Tks5$_{short}$+β from 0.89 ± 0.25 to 2.14 ± 0.96 after 5 d of differentiation (Fig. S2 A).

The regulation of myoblast differentiation has been intensively studied, and MyoD and myogenin are the best-known transcription factors governing this process (Almada and Wagers, 2016). Analyzing the chromatin immunoprecipitation sequencing database in the UCSC genome browser (Kent et al., 2002), we noticed that MyoD and myogenin bind to SH3PXD2A (the gene name of Tks5) in a differentiation-dependent manner. In parallel, we noticed five consensus E-box sequences, CANNTG, which MyoD and myogenin may bind to in the promoter region of Tks5α, suggesting that MyoD and myogenin may be the responsible transcription factors (Fig. S2 B). To test this, we used a dual luciferase promoter assay and found that the activity of Tks5α promoter region (−1,469 to +214) increased about twofold in day 3 differentiated myoblasts (Fig. 4 E). Furthermore, this enhancement of activity of the Tks5α promoter region was disturbed by mutation of its E-Box3 region (Figs. 4 F and S2 C). These results reveal that Tks5α is transcriptionally up-regulated during myogenesis with the E-Box3 as cis-element and probably by MyoD and myogenin.

Isoform switching of Tks5 is critical for myoblast fusion
To further examine the necessity of the Tks5 isoform switch for myoblast fusion, we overexpressed a mutant Tks5α with
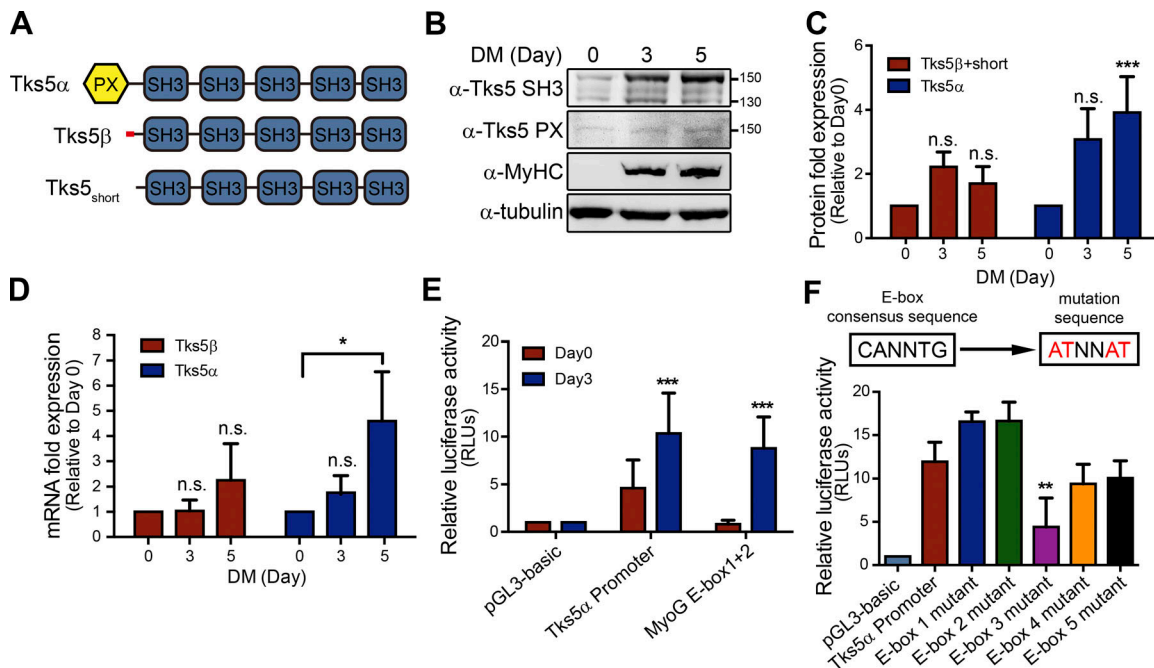
Figure 4. **Tks5 undergoes isoform switch during myoblast differentiation. (A)** Domain structure of different Tks5 isoforms. Red box represents exon 6β, which is unique in Tks5β. **(B–D)** The expression of Tks5 isoforms during myogenesis. Expression of protein or mRNA levels of different Tks5 isoforms in myoblasts upon differentiation were examined with immunoblotting (B and C) or quantitative PCR (D). C was derived from the results using anti-SH3 antibody. **(E)** Promoter activity of Tks5α promoter upon myoblast differentiation. Dual luciferase reporter assay of Tks5α promoter was performed and compared among day 0 or 3 differentiated C2C12. The MyoG E-box serves as positive control. **(F)** Dual luciferase reporter assay of different E-box mutations of Tks5α promoter. Data were analyzed with one-way ANOVA (C, D, and F) or Student's t test (E). *, $P < 0.05$; **, $P < 0.01$; ***, $P < 0.001$.

PX-domain truncation (Tks5αΔPX) in myoblasts to reverse the protein ratio of Tks5 isoforms and observe its effect on myoblast differentiation and fusion (Fig. 5). After differentiation, MyHC expression levels were comparable in both Tks5α- and Tks5αΔPX-expressing myoblasts, suggesting again that Tks5 is not critical for myoblast differentiation (Fig. 5 A). However, myoblast fusion efficiency was significantly enhanced in Tks5α-expressing cells but impaired in Tks5αΔPX-expressing myoblasts (Fig. 5, B and C). Interestingly, dot-shaped, invadosome-like structures that were labeled with F-actin and Cortactin could be detected in some undifferentiated myoblasts when Tks5α, but not Tks5αΔPX, was overexpressed (Fig. 5 D). Furthermore, the overexpression of Tks5αΔPX abolishes invadosome formation in differentiated myoblasts (Fig. 5 E). Together, these data demonstrate that Tks5 undergoes an isoform switch during myoblast differentiation, and that this switch is critical for invadosome formation and myoblast fusion.

Dyn2 is involved in myoblast fusion via actin binding and GTPase activities

The protein and mRNA level of Dyn2 also increased upon myoblast differentiation (Figs. 1 A and S3 A). Unlike Tks5, however, depletion of Dyn2 impaired myoblast differentiation, likely reflecting its essential role in clathrin-mediated endocytosis and preventing us from analyzing its later role in myoblast fusion by shRNA knockdown (Fig. S3 B). Therefore, to dissect whether Dyn2 directly participates in myoblast fusion, we used the small-molecule inhibitor Dynasore to acutely inhibit Dyn2 3 d after

differentiation. However, given the time course of myoblast fusion in culture, the inhibitor was still present for 24 h. Under these conditions, although the expression of MyHC was still reduced relative to control cells (Fig. S3, C and D), the cells nonetheless adopted their spindle morphology, indicative of differentiation. Importantly, inhibition of Dyn2 significantly inhibited myoblast fusion (Fig. S3 E).

To further dissect the Dyn2 requirement for myoblast fusion, we analyzed the effects of distinct dominant-negative mutations of Dyn2, including K44A (GTP hydrolysis defect), K/E (K414, 415, 419, 421, 426E, actin binding defect), E/K (E422, 434K, actin binding enhancing; Gu et al., 2010), and G537C and K562E (membrane fission defect; Chin et al., 2015), relative to WT Dyn2 by inducting their expression using a tetracycline-regulatable adenoviral vector after myoblast differentiation (Fig. 6 A). Importantly, under these conditions, the expression of MyHC was largely unaffected (Fig. S4 A). Control experiments established, similar to previous reports, that overexpression of membrane fission–defective Dyn2 perturbed clathrin-mediated endocytosis, whereas actin binding–defective mutants affected the actin organization but not transferrin uptake (Fig. S4, B–D; Gu et al., 2010; Chin et al., 2015). Interestingly, the fission-defective Dyn2 mutants, G537C and K562E, supported myoblast fusion to the same extent as WT; however, we detected a significant defect in myoblast fusion relative to WT in cells expressing either the GTP hydrolysis or actin binding–defective mutants, K44A and K/E (Fig. 6, B and C). The actin binding–enhanced mutant Dyn2E/K exhibited higher myoblast fusion efficiency relative to Dyn2WT.
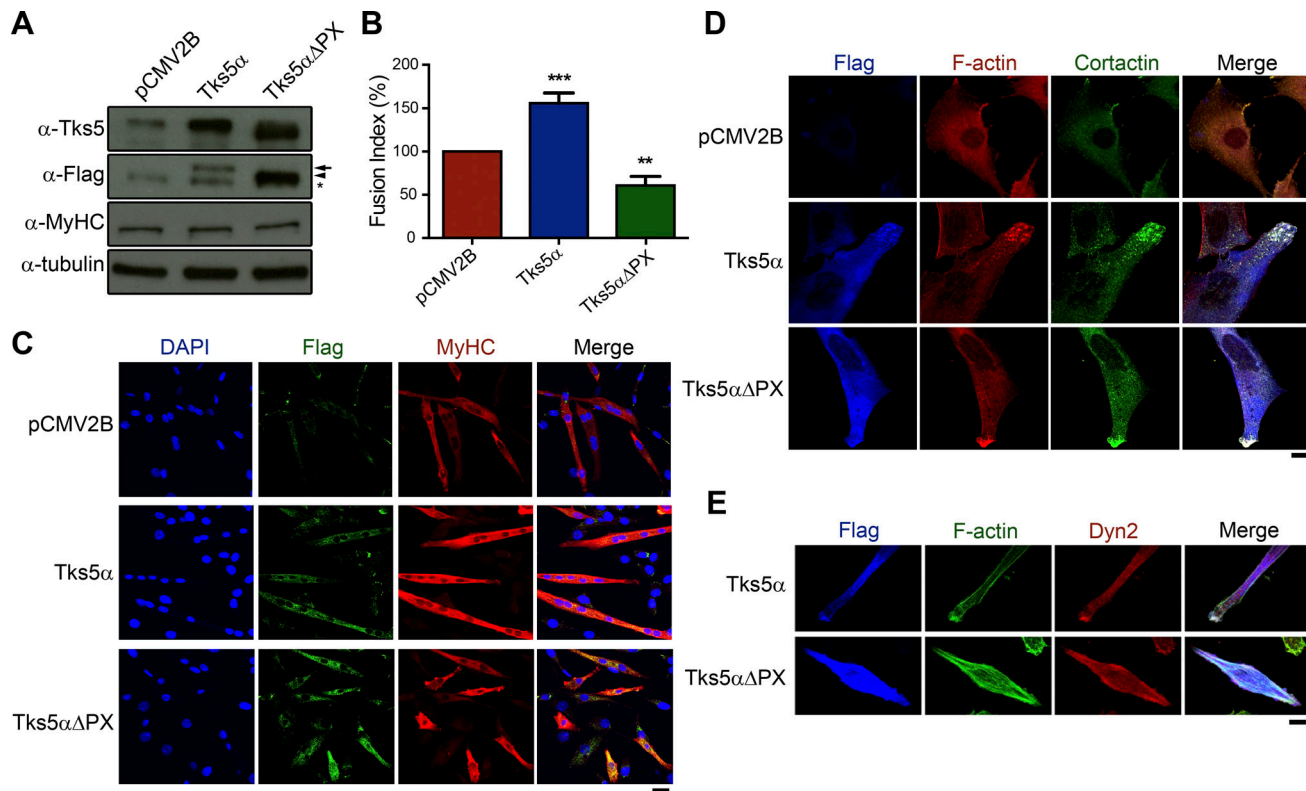
Figure 5. **Isoform switch of Tks5 is critical for myoblast fusion. (A)** Effects of ectopic expression of flag-tagged Tks5α or Tks5αΔPX in day 4 differentiated myoblasts. Cell lysates were immunoblotted with anti-Tks5 SH3 or anti-Flag antibodies, with arrow and arrowhead indicating Tks5α and Tks5αΔPX, respectively. Asterisk shows nonspecific signal of anti-Flag antibody. **(B and C)** Fusion efficiency of different Tks5 constructs expressing myoblasts. Scale bar, 30 µm. **, P < 0.01; ***, P < 0.001. **(D)** Effects of ectopic expression of flag-tagged Tks5 in undifferentiated myoblasts. After 48-h transfection, undifferentiated myoblasts were seeded on fibronectin-coated coverslips and stained for actin, Cortactin, and Flag. Maximum-intensity projections are shown. **(E)** Effects of Tks5αΔPX expression on invadosome formation. Day 3 differentiated myoblasts with Tks5α or Tks5αΔPX expression were seeded on fibronectin-coated coverslips and stained to detect endogenous Dyn2 and F-actin distribution. Scale bars, 10 µm.

Consistent with this, immunofluorescent staining showed significant reduction of the enrichment of Dyn2K44A and Dyn2K/E to the actin foci in differentiated myoblasts, although the enrichment of Dyn2E/K to the actin focus was also slightly reduced (Fig. 6, D and E). These results reveal that Dyn2 directly participates in myoblast fusion through its actin binding and GTP hydrolysis activities.

Tks5 interacts directly with Dyn2

Given the domain architecture and colocalization of Dyn2 and Tks5, we suspected they may interact through their SH3 domain and proline-rich domain (PRD), and exist in the same protein complex in myoblasts. However, we were unable to detect significant association of Tks5 and Dyn2 in myoblast lysates (not depicted), perhaps indicating that low-affinity interactions occur only when the proteins associate on the membrane. Instead, to examine their physical interaction, we used purified His-Dyn2 and GST-tagged truncated Tks5 containing no, one, or three SH3 domains as illustrated in Fig. 7 A and performed GST pulldown assays. We found that Tks5 directly interacts with Dyn2 via the first SH3 domain (GST-PX3A), and there is no significant increase of their binding affinity when additional SH3 domains are included (GST-PX3C in Fig. 7 B). From these results, we learned that Tks5 and

Dyn2 directly interact with each other, and they are both required for myoblast fusion.

Tks5 regulates Dyn2 assembly around filamentous actin

We next explored the functional significance of the Tks5–Dyn2 interaction at the actin-rich myoblast tip. We showed that Tks5 is crucial for Dyn2 localizing to invadosome (Fig. 3 B), but does Tks5 affect Dyn2 activity at the myoblast tip? Given that Dyn2 is involved in myoblast fusion through its actin binding ability, we examined the effect of Tks5 on the ability of Dyn2 to bind and assemble around actin filaments, i.e., its actin bundling activity (Gu et al., 2010). Using an F-actin bundle sedimentation assay that distinguishes individual actin filaments from larger actin bundles, we observed a prominent shift of F-actin (~50%) into the pellet upon Dyn2 addition (Fig. 7 C). Yet, adding truncated Tks5 (PX3A) into the Dyn2–F-actin mixture decreased the amount of sedimented actin from 50% to ~30%, indicating that Tks5 alters Dyn2 assembly around the actin (Fig. 7, C and D). A similar effect could also be observed when His-tagged PX3A was added into the Dyn2–F-actin bundling assay (Fig. S5, A and B).

To inspect the detailed structure of Dyn2–actin complex, we used negative stain EM and found that Dyn2 forms ring-like structures around actin (Fig. 7 E). Actin filaments were aligned
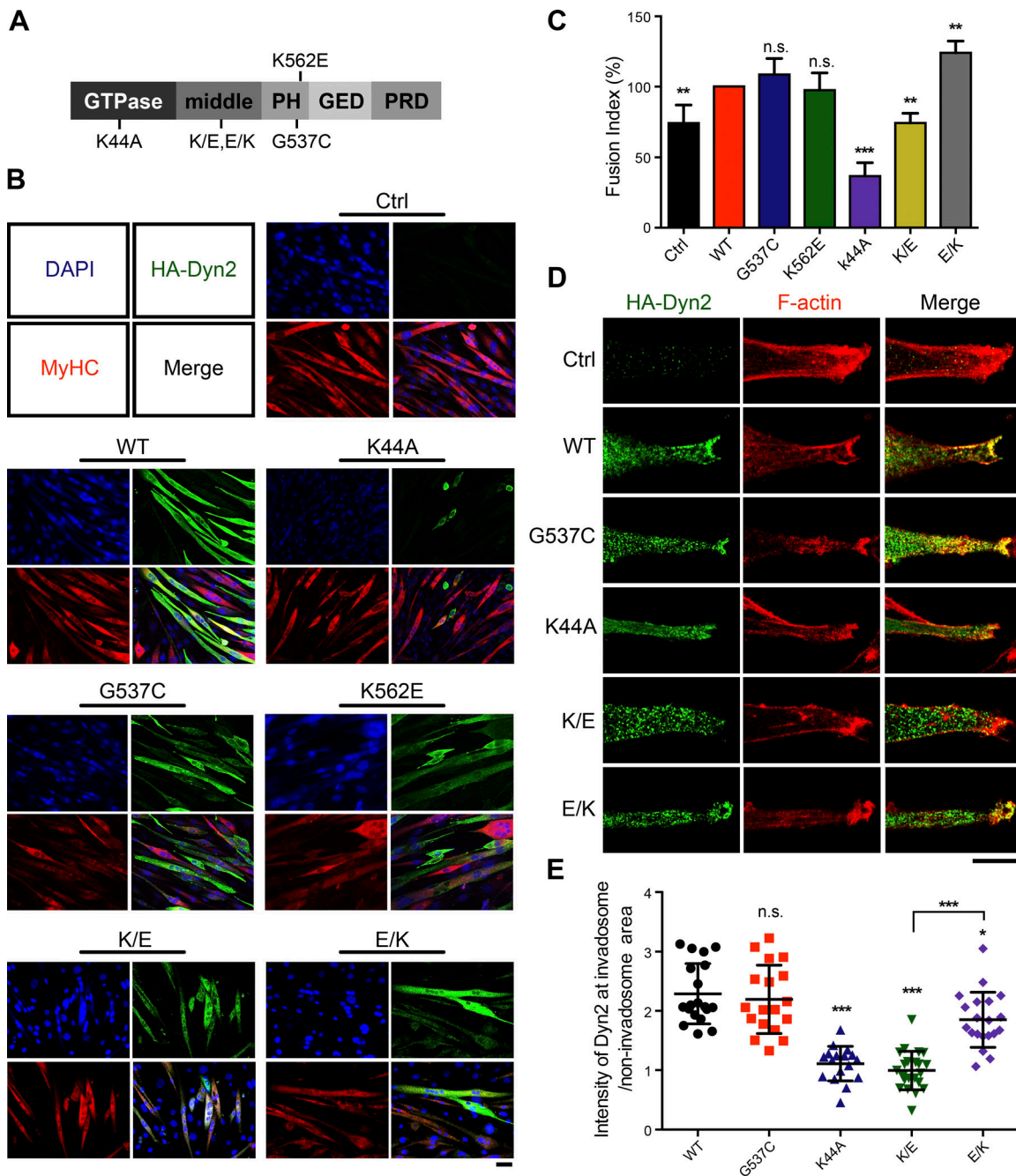
Figure 6. **Dyn2 is directly involved in myoblast fusion. (A)** Dyn2 domain structure and the mutations used in this study. **(B and C)** Fusion efficiency of myoblasts infected with different Dyn2 mutants were imaged (B) and quantified (C). These Dyn2 mutants were tetracycline-regulated and were induced 2 d after differentiation to avoid their effects on differentiation. **, P < 0.01; ***, P < 0.001. **(D and E)** Distribution of Dyn2 mutants in day 3 differentiated myoblasts. After 2 d of differentiation, C2C12 myoblasts were replated into lower density on fibronectin-coated coverslips and infected with HA-Dyn2 mutants expressing adenoviruses. After 16-h induction, Dyn2 mutants and F-actin were stained and imaged with confocal microscopy. The enrichment of Dyn2 mutants in invadosomes was quantified by the intensity of Dyn2 in actin focus divided by the intensity outside the invadosome (E). 20 cells of each mutant were analyzed. Scale bars, 10 μm.

and associated into bundles with an average diameter of 117.1 ± 33.8 nm when incubated with Dyn2. The presence of PX3A did not significantly alter these dimensions (119.8 ± 39.5 nm; Fig. 7 F). However, we observed that Dyn2 helixes align better and seem to assemble into larger spirals, which is reminiscent of dynamin helical structure on lipid nanotubes (Stowell et al., 1999; Liu et al., 2011), around the actin bundle in the presence

of Tks5 (Fig. 7 E, insets). To quantify this, we measured the diameter of these Dyn2 spirals and found that they increase significantly from 50.9 ± 15.6 to 118.6 ± 34.9 nm when Tks5 is present. Importantly, this effect was specific to Tsk5, as the SH3 domain from another Dyn2 binding partner at CCPs, Amphiphysin II, had little effect on Dyn2–actin bundle sedimentation or morphology (Fig. 7 G and Fig. 8, A–C).
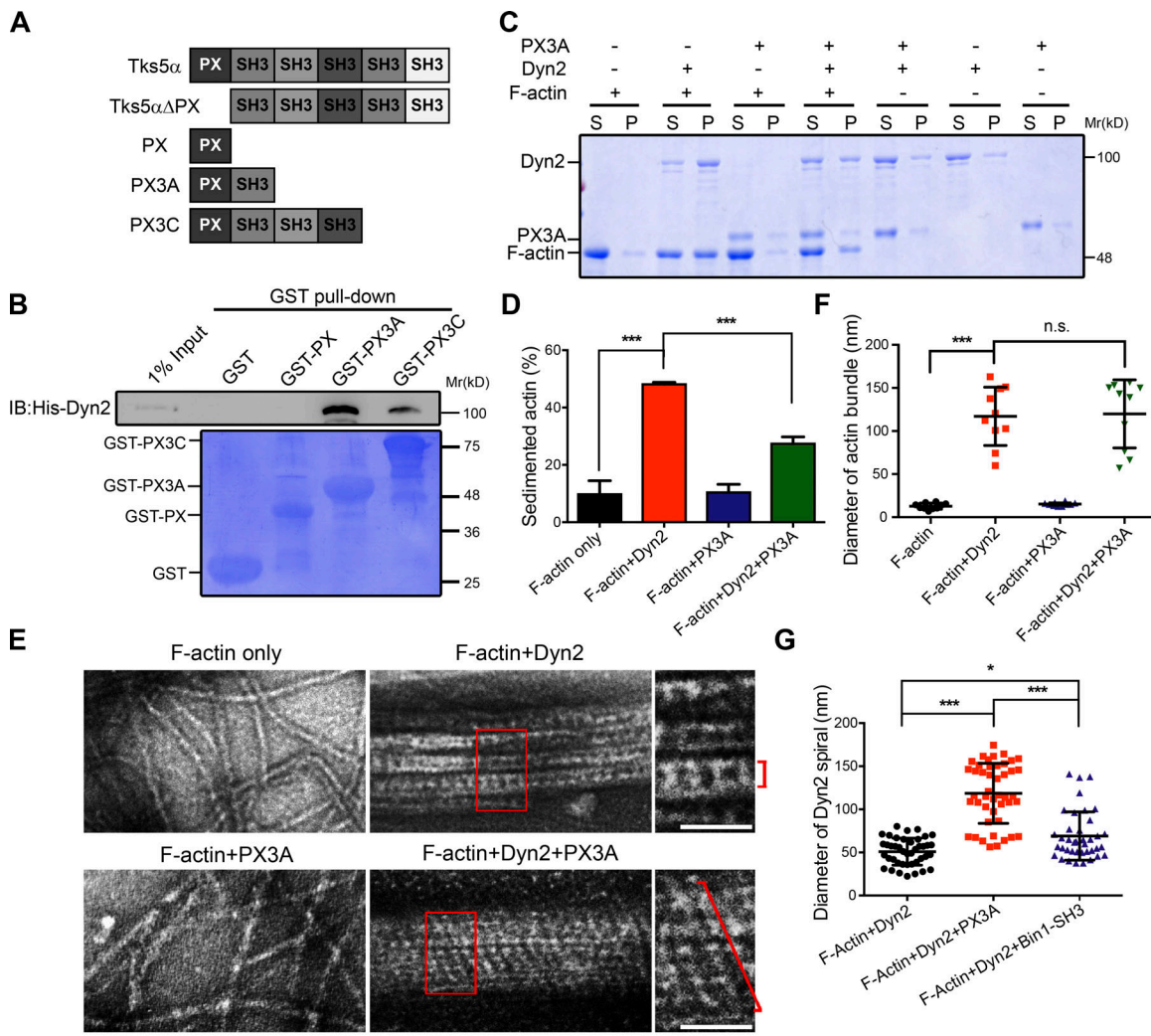
Figure 7. **Tks5 interacts with Dyn2 and regulates its assembly around actin. (A)** Domain structure of different Tks5 constructs used in this study. **(B)** Direct interaction between Dyn2 and Tks5. GST pulldown assay was performed using purified full-length Dyn2 and three GST-tagged Tks5 fragments, GST-PX, GST-PX3A, and PX3C. Bound His-Dyn2 was detected with immunoblotting, and GST-tagged proteins were shown with Coomassie Blue stain. **(C and D)** F-actin bundling assay. Prepolymerized filamentous actin was incubated with purified Dyn2 or Tks5 as indicated. After 30 min of incubation, bundled actin was sedimented into pellet (P), and the ratio of bundled actin (pellet/total) was quantified with SDS-PAGE, Coomassie Blue staining, and ImageJ (D). **(E and G)** Electron micrographs of Dyn2-mediated actin bundling with or without Tks5. Single Dyn2 spiral was indicated by red braces in the magnified panels, and the diameters of actin bundles or Dyn2 spirals in the presence or absence of Tks5 were quantified with ImageJ (F and G). Black bar, 100 nm. White bars, 50 nm. *, P < 0.05; ***, P < 0.001.

We next used immunogold EM to observe the distribution of Tks5–PX3A on Dyn2-actin bundles. While no gold particle was observed in the Dyn2-actin bundles, there were several gold particles surrounding the Tks5–PX3A–Dyn2–actin complex along the Dyn2 helixes (Fig. 8 D). To carefully examine the distribution/organization of Dyn2 in invadosomes, we used confocal, confocal equipped with Airyscan, or stimulated emission depletion (STED) microscopy to image the distribution of endogenous Dyn2 in differentiated C2C12. Consistent with our in vitro data, we observed a distinct spiral pattern of Dyn2 signal around the actin core of the invadosome, with Tks5 sometimes decorated at the tip (Fig. 8 E). These results reveal that Tks5 binds to Dyn2 and regulates its assembly into larger spirals around actin filaments both in vitro and in invadosomes.

Tks5 affects the biochemical and mechanical properties of Dyn2–actin bundles

From these results, we hypothesize that Tks5 helps Dyn2 to form larger actin bundles, allowing the invadosome to function as a molecular drill to invade the receiving myoblast. We thus wondered whether Tks5 would affect the biochemical or mechanical properties of Dyn2-bundled actin.

The GTPase activity of Dyn2 is stimulated by self-assembly (Warnock et al., 1996; Antonny et al., 2016). We therefore measured the rate of GTP hydrolysis in preassembled Dyn2-actin bundles with or without Tks5-PX3A. Interestingly, the GTP hydrolysis rate did not increase when Dyn2 formed rings around actin filaments (Fig. S5 C). However, GTP hydrolysis was significantly enhanced, by 30%, in the presence of Tks5,
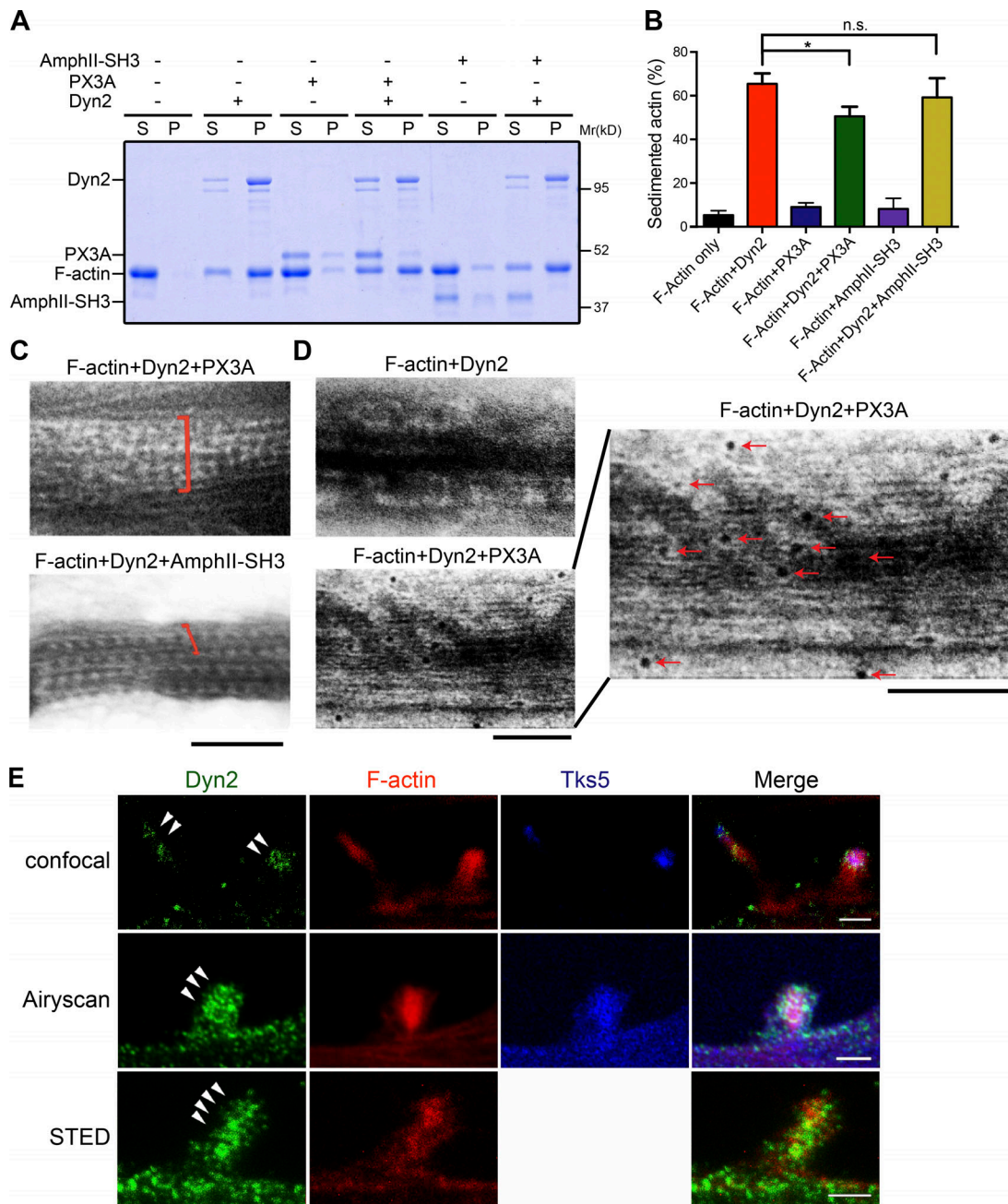
Figure 8. Tks5 regulates Dyn2 assembly around actin. (A–C) Effects of Amphiphysin II and Tks5 on Dyn2-actin bundle. SH3 domain from Tks5 (PX3A) or Amphiphysin II (AmphII-SH3) were added into Dyn2 and actin filament reactions. Bundled actin was sedimented, and the ratio of bundled actin (pellet/total) was analyzed and quantified with ImageJ (B) or imaged with negative stain TEM (C). **(D)** Immunogold staining for Tks5 on Dyn2-actin bundle. Tks5/GST-PX3A was labeled with anti-GST antibody and subsequently with 6 nm gold particle–conjugated anti-rabbit antibody. A magnified image was shown with red arrows indicating the gold particles. Scale bars, 100 nm. **(E)** Distribution of endogenous Dyn2 in invadosome. Differentiated myoblasts were stained with indicated antibodies and imaged with confocal, confocal with Airyscan detector, or STED microscopy. Single focal images are shown. Scale bars, 2 µm. *, P < 0.05.

indicating that Dyn2 spirals formed in the presence of Tks5 are better positioned for GTPase activation.

Next, we investigated whether Tks5 affects the mechanical properties of the Dyn2-actin bundle. For this, we used atomic force microscopy (AFM) to measure the topography and stiffness of the Dyn2–F-actin filament. Pre-assembled Dyn2-actin bundles formed with or without Tks5-PX3A were deposited on mica and analyzed using a recently developed, commercially available AFM surface property mapping technology, called Peakforce QNM, to measure the Dyn2-actin bundles under ambient conditions. Consistent with our EM data (Fig. 7 F), we found no difference in the height of Dyn2-actin bundles with or without Tks5-PX3A (57.6 ± 11.4 and 63.8 ± 10.4 nm, respectively; Fig. 9, A and B). However, the stiffness of Dyn2-actin bundles increased from 220.3 ± 53.9 to 433.8 ± 47.9 MPa in the presence of Tks5 (Fig. 9, C and D).
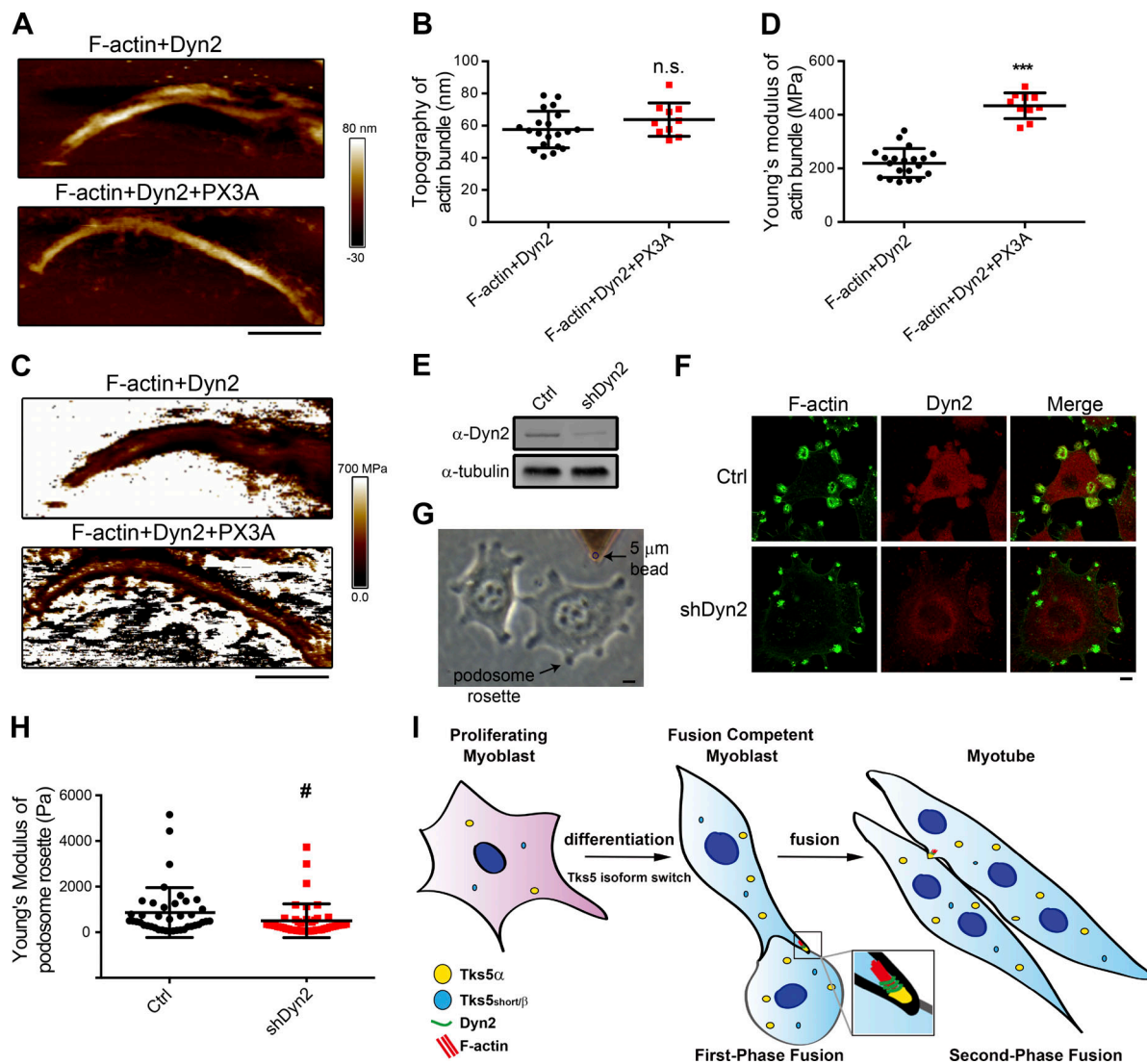
Figure 9. **Tks5 regulates the physical properties of Dyn2-actin bundles. (A–D)** AFM topography and stiffness map (Young's modulus) of Dyn2-actin bundles. Height (A) and corresponding stiffness (C) of Dyn2-actin bundles with or without GST-PX3A addition were recorded and quantified with Peakforce QNM. Quantification results are shown in C and D. $n \geq 10$. Scale bars, 800 µm. ***, $P < 0.001$. **(E and F)** Dyn2 knockdown in c-SrcY527F–transformed NIH3T3 cells. Dyn2 was depleted by lentiviral shRNA and selected with puromycin for 3 d. Cells were processed for immunoblotting (E) or immunostaining (F). Scale bar, 10 µm. **(G and H)** AFM stiffness map (Young's modulus) of podosome rosette. Podosome rosettes in control or Dyn2-depleted c-SrcY527F–transformed NIH3T3 cells with diameter ~5 µm were analyzed with AFM probe equipped with a 5-µm bead in medium (G). Approximately 40 podosome rosettes in >10 cells of each condition were measured and quantified in H. #, $P = 0.079$. **(I)** Tks5 mediates invadosome maturation through regulating dynamin-actin organization to drive myoblast fusion. Upon myoblast differentiation, Tks5 is up-regulated and undergoes isoform switching to the long isoform Tks5α that encodes a membrane-interacting PX domain. Tks5α promotes the formation and maturation of an invadosome by dictating Dyn2 assembly, strengthening the protrusive actin-rich structure and perhaps coupling these force-generating filaments to the membrane. The invadosome thus functions as a molecular drill to propel both the first- and second-phase myoblast fusion.

To examine the effect of Dyn2–Tks5 complex on invadosome rigidity in vivo, we used c-SrcY527F–transformed NIH3T3 fibroblasts that form stable and micrometer-scaled podosome rosettes which could still be observed upon 60% Dyn2 knockdown (Pan et al., 2011; Fig. 9, E and F). We thus measured the stiffness of podosome rosettes of size ~5 µm by AFM equipped with a 5-µm bead AFM probe. In line with our in vitro results, the average stiffness of podosome rosettes in Dyn2 knockdown (505.7 ± 739.9 Pa) was lower than in control cells (863.4 ± 1092 Pa), although the P value was ~0.08 (Fig. 9 G). Together, these results demonstrated that Tks5 interacts with

Dyn2 and modulates its assembly into helices around actin filaments to increase the rigidity of the actin bundle and, probably, the invadosome.

Discussion

The actin cytoskeleton is known to be the driving force for myoblast fusion from fly to mouse (Srinivas et al., 2007; Richardson et al., 2008; Abmayr and Pavlath, 2012). Here we report that actin-enriched invadosomes, formed as a consequence of isoform switching of Tks5 during myogenesis,

Chuang et al.
Dynamin-2 promotes myoblast fusion via actin bundling ability

Journal of Cell Biology 1680
https://doi.org/10.1083/jcb.201809161

underpin the acquisition of myoblast fusion competency in mammalian cells. The protrusive invadosome is formed asymmetrically in the attacking myoblast at the fusion site. Tks5 recruits Dyn2 and regulates its coassembly with actin filaments to form stiffer actin drills to invade the receiving cells and drive membrane fusion (Fig. 9 H).

Previous studies have established that Src-phosphorylation of Tks5 regulates invadosome assembly and invasion in cancer cells (Seals et al., 2005; Blouw et al., 2008). Here we reveal a second mechanism of Tks5 activation involving an isoform switch. In undifferentiated myoblasts, Tks5α activity is counteracted by two shorter isoforms preventing invadosome formation at an inappropriate stage. Upon differentiation, myogenic transcription factors up-regulate Tks5α to switch its isoform ratio, thus promoting the formation of invadosomes and driving myoblast fusion. The up-regulation of Tks5 in cultured C2C12 is consistent with the in silico analysis result of increased SH3PXD2A mRNA expression in adult regenerating myofibers upon muscle injury (GEO dataset GDS4924; Lukjanenko et al., 2013). Recently, the expression of Tks5 was reported to be regulated by changes in the intracellular metabolic environment in rheumatoid arthritis T cells to enhance their tissue infiltration ability (Shen et al., 2017). Interestingly, Tks5 was also reported to be required for the podosome formation induced by phorbol 12,13-dibutyrate in myoblasts (Thompson et al., 2008). Together, these studies reveal that transcriptional and posttranscriptional mechanisms of regulation provide sophisticated control of Tks5 activity for developmental and pathogenic regulation of cell invasive behaviors.

The existence and importance of Dyn2 in invadosomes has been known for more than a decade (Ochoa et al., 2000); however, the function of Dyn2 in invadosomes remains poorly understood. Dyn2 could promote invadosome formation through its role in endocytosis, its ability to promote actin polymerization either directly or via its interactions with actin regulators, or both (Lee and De Camilli, 2002; McNiven et al., 2004; Ferguson and De Camilli, 2012). Our data suggest a structural role for Dyn2 in the invadosome whereby Dyn2 binds and assembles around filamentous actin, forming larger, more rigid actin bundles. Notably, the stiffness of podosome rosettes measured in c-SrcY527F transformed NIH3T3 cells is much lower than the stiffness of podosomes in macrophage, 863.4 ± 1,092 versus 43,800 ± 9,300 Pa, respectively (Labernadie et al., 2010). This discrepancy may reflect the diverse physical property of different types of podosomes or potential technical issue in the analysis, for example the influence of substrate. In addition, it is worth noting that transformed or cancer cells usually have lower cell stiffness than their normal counterparts (Lin et al., 2015); thus c-SrcY527F–transformed NIH3T3 may have lower cell stiffness as well.

Structural and biophysical studies of assembled dynamin have focused on its powerstroke and GTPase-dependent ability to squeeze membranes (Chappie et al., 2011; Morlot et al., 2012; Reubold et al., 2015). Thus, it is tempting to hypothesize that Dyn2 might also squeeze actin filaments to help them align and tighten up by assembling into large spirals and then further constricting them as a result of GTP-hydrolysis–induced conformational changes and/or ratcheting (Antonny et al., 2016). Therefore, using a similar principle, albeit on different templates, Dyn2 could promote membrane fission during endocytosis or membrane fusion during myogenesis. These diverse functions of Dyn2 are dictated by its interaction with diverse SH3-domain–containing binding partners within the cell. The SH3–PRD interaction not only recruits dynamin to its site of action but also regulates its assembly. The SH3 domains from different proteins have distinct effects on dynamin oligomerization. Whereas Grb2, intersectin-1, and SNX9 facilitate dynamin oligomerization, Amphiphysin I and II prevent dynamin oligomerization in solution (Owen et al., 1998; Soulet et al., 2005; Knezevic et al., 2011). Here we show that Tks5 alters Dyn2 assembly on actin filaments to create more regular Dyn2-scaffolds, position Dyn2 for improved assembly-stimulated GTPase activity, and as a consequence, increase the rigidity of the actin-Dyn2 bundles.

The asymmetry of the actin cytoskeleton and the subsequent mechanical forces they generate in myoblast fusion has been beautifully examined in Drosophila muscle development (Chernomordik and Kozlov, 2015; Kim et al., 2015b; Duan et al., 2018). While similar actin asymmetry is observed in mammalian myoblast fusion, the cytoskeleton asymmetry is actin specific while microtubules are equally distributed among two fusing myoblasts. Furthermore, Dyn2 is also asymmetrically distributed in two fusing myoblasts such that it is enriched together with actin at the membrane protrusion in the attacking cell, whereas it colocalized better with AP-2 at the membrane periphery in the receiving cell (Fig. 1 F). The differential distribution of Dyn2 is in line with current understanding of myoblast fusion that the attacking cell applies protrusive force while the receiving cell exerts resistance force to generate close membrane apposition and tension that ultimately drives membrane fusion.

Our results provide a missing piece to the puzzle that reveals the evolutionarily conserved molecular mechanism for myoblast fusion. Although Drosophila does not encode Tks5, the fly utilizes a podosome-like structure to provide the invasive force for myoblasts to protrude and fuse with myotubes (Sens et al., 2010). Similarly, there is only one dynamin encoded by the fly genome, shibire, which is highly expressed in the nervous system. Intriguingly, shibire is also critical for myoblast fusion in the Drosophila embryo (unpublished data; Antonny et al., 2016). Together, these findings suggest that myoblast fusion is an evolutionarily conserved process using dynamin- and actin-based membrane protrusions to drive membrane fusion. Despite the importance and multiple functions of invadosomes in human health and disease, little is known about the evolution of invadosomes and their regulation in most tissues under physiological or developmental conditions. Our findings reveal the regulation of invadosome formation in muscle development and pave the way for future studies of the versatile functions and sophisticated regulation of invadosomes in different tissues and developmental stages.

Materials and methods
Cell culture, transfection, and lentiviral and adenoviral infection
Mouse-derived C2C12 myoblasts (ATTC; CRL-1772) were cultured in growth medium (GM; DMEM supplemented with 2 mM

Chuang et al.
Dynamin-2 promotes myoblast fusion via actin bundling ability

Journal of Cell Biology 1681
https://doi.org/10.1083/jcb.201809161

L-glutamine, 1 mM sodium pyruvate, antibiotics, and 10% FBS [Gibco]). To induce differentiation, C2C12 were seeded onto fibronectin-coated plates or coverslips in GM, grown to 90% confluence, and then switched to DM (same as GM but with 2% horse serum [Gibco]). This time point was considered day 0 of differentiation. c-SrcY527F–transformed NIH3T3 cells were cultured in DMEM, 10% FBS, and 200 µg/ml Hygromycin B as previously described (Pan et al., 2011).

For transfection, cells at 70% confluence were transfected with interested DNA using Lipofectamine 2000 (Invitrogen), as recommended by the manufacturer. For lentiviral infection, 50% confluent myoblasts or c-SrcY527F–transformed NIH3T3 were infected with viruses together with 8 µg/ml polybrene and selected with 2 µg/ml puromycin for 3 d followed by DM treatment. For adenoviral infection, 50% confluent myoblasts were infected with viruses in the presence of 1 µg/ml tetracycline to suppress protein expression. Once the infected cells reached confluence, the medium was changed to DM containing 1 µg/ml tetracycline. After differentiation for 48 h, tetracycline was lowered to 20 ng/ml, and the fusion efficiency or protein distribution was analyzed with immunofluorescent staining. For pCMV2b construct transfection, Lipofectamine 3000 (Invitrogen) was used for better transfection efficiency, and cells were selected with 2 mg/ml G418 for 2 d before DM replacement.

Molecular biology
For Dyn2 expression and purification, human dynamin-2 was constructed into pIEX6 (Novagen) for expression in insect cell Sf9 or adenoviral vector pADtet for expression in mammalian cells as previously described (Chin et al., 2015). For Tks5 expression, human Tks5 (SH3PXD2A) were cloned into pCMV2b or pGEX4T-1 for expression in mammalian cells or *Escherichia coli*, respectively. Plasmids used in this study are listed in Table S1. Lentiviral shRNA was generated and performed as described previously (Gu et al., 2010), and the targeted sequences are listed in Table S2. Quantitative PCR was performed as previously described (Chen et al., 2016), and primers are listed in Table S3. For Tks5 promoter construction, a DNA fragment containing –1,469 to approximately +214 base pairs of Tks5α transcription start site was synthesized, sequence-checked, and subcloned into pGL3-basic (Promega). E-box mutations were introduced by site-directed mutagenesis with primers listed in Table S3.

Immunofluorescent staining and imaging
For indirect immunofluorescence staining, cells were fixed with 4% formaldehyde and permeabilized with 0.1% saponin. After blocking with 3% BSA and 5% normal donkey serum, cells were stained with the indicated primary and secondary antibodies. Samples were observed under confocal microscope LSM700 with 20× Plan-Apochromat (NA) or 63×, 1.35-NA oil-immersion objective (Carl Zeiss), LSM880 with Airyscan detector (Carl Zeiss), or TSC SP8 X STED 3X (Leica) with 100× oil objective 1.4 NA (STED microscopy). Samples were acquired with excitation laser at 594 nm, depletion laser at 660 nm, and a Hybrid Detector (Leica HyD).

Antibodies used are listed in Table S4. For time-lapse microscopy, 48-h differentiated myoblasts were lifted with trypsin, and half of the cells were replated on fibronectin-coated glass-bottom dishes to have proper cell density. Cells were placed in imaging medium (phenol-red free DM with 20 mM Hepes, pH 7.4, 50 µg/ml ascorbic acid, and 10% FBS) at 37°C, and images were acquired with Zeiss inverted microscopy Axio Observer Z1 with time interval 5 min for >5 h.

Matrix degradation assay
Day 3 differentiated C2C12 myoblasts were plated on glass coverslips coated with 20 ng/ml FITC-conjugated gelatin (Invitrogen) as previously described (Pan et al., 2011). After 24 h, the cells were fixed, stained for F-actin, and imaged with confocal microscopy.

Cell fusion assay
To quantify the efficiency of myoblast fusion, day 4 or 5 differentiated myoblasts were fixed and stained with DAPI and indicated antibodies. Images were taken on a confocal microscope LSM700 with a 20× Plan-Apochromat objective lens. We prepared and analyzed images using ZEN 2009 (Carl Zeiss). For each condition, 10–20 randomly chosen fields of view (the total numbers of nuclei per condition averaged ∼300–500) were analyzed. The efficiency of myoblast fusion was quantified as the percentage of cell nuclei in multinucleated cells (≥3 nuclei in one cell). To minimize the effect of differentiation, we scored only nuclei in MyHC-positive cells.

Dual-luciferase reporter assay
The promoter reporter assay was performed according to the technical manual. In brief, C2C12 cells were seeded in six-well plates before being cotransfected (at 70% confluence) with the indicated reporter constructs using Lipofectamine 3000 (Invitrogen). After 2-d incubation or 3-d differentiation, luciferase activity was measured by a Dual-Glo Luciferase Assay System as recommended by the manufacturer (Promega). The relative light units were firefly luciferase units normalized to the coexpressed Renilla luciferase.

Transferrin uptake assay
Transferrin internalization was performed as previously described (Liu et al., 2008). Briefly, indicated virus-infected myoblasts on coverslips were incubated with 5 µg/ml Alexa Fluor 488–conjugated transferrin for 10 min at 37°C. Cells were washed extensively with cold PBS and acid buffer (150 mM NaCl and 150 mM glycine, pH 2.0), and then fixed and stained with anti-HA antibody. After immunostaining and mounting, cells were viewed and imaged with confocal microscopy.

Protein purification and GST pulldown assay
Dynamin proteins were expressed in Sf9 cells transiently transfected with various constructs and purified as previously described (Liu et al., 2011). GST-PX, GST-PX3A, GST-PX3C, and GST-AmphII-SH3 were expressed in *E. coli* and were purified with glutathione Sepharose beads and eluted as suggested by the manufacturer (GE).

For GST pulldown assay, 40 µg of GST or GST-Tks5 immobilized on glutathione beads was incubated with purified 2 µg

Chuang et al.
Dynamin-2 promotes myoblast fusion via actin bundling ability

Journal of Cell Biology 1682
https://doi.org/10.1083/jcb.201809161

His-Dyn2 protein in 1 ml binding buffer (PBS with 1 mM DTT, 10% glycerol, and 1% Tween-20) at 4°C for 1 h. After three washes with binding buffer containing 1.2% Tween-20, bound proteins were detected by Western blotting.

F-actin bundle sedimentation assay

The actin bundling assay was performed as described previously (Gu et al., 2010) with a few modifications. Briefly, 10 µM purified rabbit skeletal muscle actin (Cytoskeleton) was diluted in general actin buffer (5 mM Tris, pH 7.4, 0.2 mM ATP, 0.2 mM CaCl$_2$, and 0.5 mM DTT) and incubated at 4°C for 1 h and centrifuged at 20,000 g for 15 min to remove aggregated proteins. The G-actin was polymerized by the addition of 50 mM KCl, 2 mM MgCl$_2$, and 1 mM ATP for 1 h at room temperature. 5 µM polymerized F-actin was incubated with 1 µM Dyn2 or 1 µM Tks5-PX3A in actin polymerization buffer (2.5 mM Tris, pH 7.4, 0.1 mM CaCl$_2$, 0.25 mM DTT, 50 mM KCl, 2 mM MgCl$_2$, and 1 mM ATP) for 30 min at room temperature. The mixture was centrifuged at 14,000 g for 20 min at room temperature. Protein in supernatants and pellets were solubilized in SDS sample buffer and subjected to SDS-PAGE. Proteins were visualized by Coomassie blue staining, and band intensities were quantified using ImageJ (National Institutes of Health).

Transmission EM

To visualize actin bundled by Dyn2, 5 µM filamentous actin was incubated with or without 1 µM Dyn2 and 1 µM Tks5-PX3A at room temperature for 30 min. The mixture was then adsorbed onto carbon-coated, glow-discharged grids and stained with 2% uranyl acetate. Images were collected using a Hitachi H-7650 EM at 75 kV and a nominal magnification of 120,000. For immunogold labeling, actin bundles made as described above were absorbed onto carbon-coated, glow-discharged nickel grids and blocked (1% BSA in HCB100 buffer: 20 mM Hepes, pH 7.4, 2 mM EGTA, 100 mM NaCl, 1 mM MgCl$_2$, and 1 mM ATP) for 60 min at 4°C. Grids were stained with the primary antibody against GST for 90 min at 4°C. After HCB100 buffer wash, grids were incubated with secondary antibodies for another 60 min at 4°C and 2% uranyl acetate staining after washing.

GTPase activity assay

Purified Dyn2 (1 µM) and actin (5 µM) bundles were prepared as described above for 30-min incubation at room temperature with or without Tks5-PX3A. After warming up these reactions to 37°C, GTP was added to each reaction to reach 1 mM with pipetting, and GTP hydrolysis was measured as a function of time using a colorimetric malachite green assay that detects the release of inorganic phosphate (Leonard et al., 2005).

AFM

For measurements of the topography and stiffness of actin bundles, a BioScope Resolve BioAFM (Bruker) equipped with rectangular silicon cantilevers with sharpened tetrahedral tips (ARROW-FM-20 Nanoworld) was used as previously described (Ohniwa et al., 2013) with a few modifications. These probes had a tip radius range within 15–60 nm, a resonant frequency of ~75 kHz, and a spring constant of ~2.8 N/m. Before each

measurement, the spring constants and tip radius of cantilevers were calibrated via relative thermal tune method. The microscope was operated in the Peak Force QNM Mode at a scanning rate of 1 Hz. The PeakForce setpoint (indenting force) was manually adjusted to keep deformation at 5 nm. Force–distance curves were collected and calculated with the Bruker package software NanoScope Analysis based on the DMT model (Sweers et al., 2011).

To measure the stiffness of podosome rosettes in a cell, a JPK nanoWizard II AFM with BioCell (JPK Instruments) was used as previously described (Lin et al., 2015) with a few modifications. Briefly, a tipless cantilever (Arrow-TL1-50, Nanoworld) equipped with a 5-µm-diameter polystyrene bead was used. The spring constant of cantilever was calibrated via thermal noise method in medium before each measurement and ranged within 0.04–0.06 N/m. We used 0.5 nN indentation force, and the force–distance curves and Young's modulus were performed and calculated with the JPK package software based on the Hertz model (Labernadie et al., 2010). Specifically, indentation depth was restricted to 50–300 nm to avoid influence of the substrate.

To prepare samples for AFM, actin bundles were prepared as for EM imaging and deposited onto plain mica by 5-min incubation. After removal of unbound materials and air drying, AFM topography and DMT modulus maps were acquired in ambient environment. To measure the stiffness of invadosome, c-SrcY527F–transformed NIH3T3 cells were infected with control or shDyn2 viruses and selected with puromycin for 3 d. Cells were seeded on uncoated dishes at 50% confluence 1 d before AFM analysis.

Statistical analysis

Quantitative data were expressed as mean ± SD of at least three independent experiments. All data were analyzed with one-way ANOVA, except the dual luciferase reporter assay on Tks5α promoter upon differentiation and AFM data, which were analyzed with Student's t test. $P < 0.05$ was considered statistically significant, indicated as *, $P < 0.05$; **, $P < 0.01$; and ***, $P < 0.001$.

Online supplemental material

Fig. S1 shows the distribution of Dyn2 and Tks5 in myoblasts. Fig. S2 displays the promoter sequences of Tks5 and the protein ratio of Tks5 isoforms during myoblast differentiation. Fig. S3 exhibits the effect of Dyn2 knockdown on myogenesis. Fig. S4 exhibits the effects of Dyn2 mutants on endocytosis and actin organization in myoblasts. Fig. S5 illustrates the effects of SH3 domain on Dyn2-actin bundles. Table S1 shows the plasmids used in this study. Tables S2 and S3 list shRNA and primers used in this study. Table S4 describes the antibodies used in the study. Video 1 shows the distribution of Dyn2-GFP during myoblast fusion.

References

Abmayr, S.M., and G.K. Pavlath. 2012. Myoblast fusion: lessons from flies and mice. *Development.* 139:641–656. https://doi.org/10.1242/dev.068353

Albiges-Rizo, C., O. Destaing, B. Fourcade, E. Planus, and M.R. Block. 2009. Actin machinery and mechanosensitivity in invadopodia, podosomes and focal adhesions. *J. Cell Sci.* 122:3037–3049. https://doi.org/10.1242/jcs.052704

Almada, A.E., and A.J. Wagers. 2016. Molecular circuitry of stem cell fate in skeletal muscle regeneration, ageing and disease. *Nat. Rev. Mol. Cell Biol.* 17:267–279. https://doi.org/10.1038/nrm.2016.7

Antonny, B., C. Burd, P. De Camilli, E. Chen, O. Daumke, K. Faelber, M. Ford, V.A. Frolov, A. Frost, J.E. Hinshaw, et al. 2016. Membrane fission by dynamin: what we know and what we need to know. *EMBO J.* 35:2270–2284. https://doi.org/10.15252/embj.201694613

Blau, H.M., G.K. Pavlath, E.C. Hardeman, C.P. Chiu, L. Silberstein, S.G. Webster, S.C. Miller, and C. Webster. 1985. Plasticity of the differentiated state. *Science.* 230:758–766. https://doi.org/10.1126/science.2414846

Blouw, B., D.F. Seals, I. Pass, B. Diaz, and S.A. Courtneidge. 2008. A role for the podosome/invadopodia scaffold protein Tks5 in tumor growth in vivo. *Eur. J. Cell Biol.* 87:555–567. https://doi.org/10.1016/j.ejcb.2008.02.008

Cejudo-Martin, P., A. Yuen, N. Vlahovich, P. Lock, S.A. Courtneidge, and B. Díaz. 2014. Genetic disruption of the sh3pxd2a gene reveals an essential role in mouse development and the existence of a novel isoform of tks5. *PLoS One.* 9:e107674. https://doi.org/10.1371/journal.pone.0107674

Chappie, J.S., J.A. Mears, S. Fang, M. Leonard, S.L. Schmid, R.A. Milligan, J.E. Hinshaw, and F. Dyda. 2011. A pseudoatomic model of the dynamin polymer identifies a hydrolysis-dependent powerstroke. *Cell.* 147:209–222. https://doi.org/10.1016/j.cell.2011.09.003

Chen, E.H., and E.N. Olson. 2005. Unveiling the mechanisms of cell-cell fusion. *Science.* 308:369–373. https://doi.org/10.1126/science.1104799

Chen, E.H., E. Grote, W. Mohler, and A. Vignery. 2007. Cell-cell fusion. *FEBS Lett.* 581:2181–2193. https://doi.org/10.1016/j.febslet.2007.03.033

Chen, Y.C., H.J. Chen, W.C. Tseng, J.M. Hsu, T.T. Huang, C.H. Chen, and C.L. Pan. 2016. A C. elegans Thermosensory Circuit Regulates Longevity through crh-1/CREB-Dependent flp-6 Neuropeptide Signaling. *Dev. Cell.* 39:209–223. https://doi.org/10.1016/j.devcel.2016.08.021

Chernomordik, L.V., and M.M. Kozlov. 2015. Myoblast fusion: playing hard to get. *Dev. Cell.* 32:529–530. https://doi.org/10.1016/j.devcel.2015.02.018

Chin, Y.H., A. Lee, H.W. Kan, J. Laiman, M.C. Chuang, S.T. Hsieh, and Y.W. Liu. 2015. Dynamin-2 mutations associated with centronuclear myopathy are hypermorphic and lead to T-tubule fragmentation. *Hum. Mol. Genet.* 24:5542–5554. https://doi.org/10.1093/hmg/ddv285

Duan, R., J.H. Kim, K. Shilagardi, E.S. Schiffhauer, D.M. Lee, S. Son, S. Li, C. Thomas, T. Luo, D.A. Fletcher, et al. 2018. Spectrin is a mechanoresponsive protein shaping fusogenic synapse architecture during myoblast fusion. *Nat. Cell Biol.* 20:688–698. https://doi.org/10.1038/s41556-018-0106-3

Ferguson, S.M., and P. De Camilli. 2012. Dynamin, a membrane-remodelling GTPase. *Nat. Rev. Mol. Cell Biol.* 13:75–88. https://doi.org/10.1038/nrm3266

Gu, C., S. Yaddanapudi, A. Weins, T. Osborn, J. Reiser, M. Pollak, J. Hartwig, and S. Sever. 2010. Direct dynamin-actin interactions regulate the actin cytoskeleton. *EMBO J.* 29:3593–3606. https://doi.org/10.1038/emboj.2010.249

Jahn, R., and D. Fasshauer. 2012. Molecular machines governing exocytosis of synaptic vesicles. *Nature.* 490:201–207. https://doi.org/10.1038/nature11320

Kent, W.J., C.W. Sugnet, T.S. Furey, K.M. Roskin, T.H. Pringle, A.M. Zahler, and D. Haussler. 2002. The human genome browser at UCSC. *Genome Res.* 12:996–1006. https://doi.org/10.1101/gr.229102

Kim, J.H., P. Jin, R. Duan, and E.H. Chen. 2015a. Mechanisms of myoblast fusion during muscle development. *Curr. Opin. Genet. Dev.* 32:162–170. https://doi.org/10.1016/j.gde.2015.03.006

Kim, J.H., Y. Ren, W.P. Ng, S. Li, S. Son, Y.S. Kee, S. Zhang, G. Zhang, D.A. Fletcher, D.N. Robinson, and E.H. Chen. 2015b. Mechanical tension drives cell membrane fusion. *Dev. Cell.* 32:561–573. https://doi.org/10.1016/j.devcel.2015.01.005

Knezevic, I., D. Predescu, C. Bardita, M. Wang, T. Sharma, B. Keith, R. Neamu, A.B. Malik, and S. Predescu. 2011. Regulation of dynamin-2 assembly-disassembly and function through the SH3A domain of intersectin-1s. *J. Cell. Mol. Med.* 15:2364–2376. https://doi.org/10.1111/j.1582-4934.2010.01226.x

Kozlov, M.M., and L.V. Chernomordik. 2015. Membrane tension and membrane fusion. *Curr. Opin. Struct. Biol.* 33:61–67. https://doi.org/10.1016/j.sbi.2015.07.010

Kozlovsky, Y., and M.M. Kozlov. 2002. Stalk model of membrane fusion: solution of energy crisis. *Biophys. J.* 82:882–895. https://doi.org/10.1016/S0006-3495(02)75450-7

Labernadie, A., C. Thibault, C. Vieu, I. Maridonneau-Parini, and G.M. Charrière. 2010. Dynamics of podosome stiffness revealed by atomic force microscopy. *Proc. Natl. Acad. Sci. USA.* 107:21016–21021. https://doi.org/10.1073/pnas.1007835107

Lee, E., and P. De Camilli. 2002. Dynamin at actin tails. *Proc. Natl. Acad. Sci. USA.* 99:161–166. https://doi.org/10.1073/pnas.012607799

Leikina, E., K. Melikov, S. Sanyal, S.K. Verma, B. Eun, C. Gebert, K. Pfeifer, V.A. Lizunov, M.M. Kozlov, and L.V. Chernomordik. 2013. Extracellular annexins and dynamin are important for sequential steps in myoblast fusion. *J. Cell Biol.* 200:109–123. https://doi.org/10.1083/jcb.201207012

Leonard, M., B.D. Song, R. Ramachandran, and S.L. Schmid. 2005. Robust colorimetric assays for dynamin's basal and stimulated GTPase activities. *Methods Enzymol.* 404:490–503. https://doi.org/10.1016/S0076-6879(05)04043-7

Li, C.M., G. Chen, T.L. Dayton, S. Kim-Kiselak, S. Hoersch, C.A. Whittaker, R.T. Bronson, D.G. Beer, M.M. Winslow, and T. Jacks. 2013. Differential Tks5 isoform expression contributes to metastatic invasion of lung adenocarcinoma. *Genes Dev.* 27:1557–1567. https://doi.org/10.1101/gad.222745.113

Lin, H.H., H.K. Lin, I.H. Lin, Y.W. Chiou, H.W. Chen, C.Y. Liu, H.I. Harn, W.T. Chiu, Y.K. Wang, M.R. Shen, and M.J. Tang. 2015. Mechanical phenotype of cancer cells: cell softening and loss of stiffness sensing. *Oncotarget.* 6:20946–20958.

Linder, S., and C. Wiesner. 2015. Tools of the trade: podosomes as multipurpose organelles of monocytic cells. *Cell. Mol. Life Sci.* 72:121–135. https://doi.org/10.1007/s00018-014-1731-z

Liu, Y.W., M.C. Surka, T. Schroeter, V. Lukiyanchuk, and S.L. Schmid. 2008. Isoform and splice-variant specific functions of dynamin-2 revealed by analysis of conditional knock-out cells. *Mol. Biol. Cell.* 19:5347–5359. https://doi.org/10.1091/mbc.e08-08-0890

Liu, Y.W., S. Neumann, R. Ramachandran, S.M. Ferguson, T.J. Pucadyil, and S.L. Schmid. 2011. Differential curvature sensing and generating activities of dynamin isoforms provide opportunities for tissue-specific regulation. *Proc. Natl. Acad. Sci. USA.* 108:E234–E242. https://doi.org/10.1073/pnas.1102710108

Lukjanenko, L., S. Brachat, E. Pierrel, E. Lach-Trifilieff, and J.N. Feige. 2013. Genomic profiling reveals that transient adipogenic activation is a hallmark of mouse models of skeletal muscle regeneration. *PLoS One.* 8:e71084. https://doi.org/10.1371/journal.pone.0071084

McMahon, H.T., M.M. Kozlov, and S. Martens. 2010. Membrane curvature in synaptic vesicle fusion and beyond. *Cell.* 140:601–605. https://doi.org/10.1016/j.cell.2010.02.017

McNiven, M.A., M. Baldassarre, and R. Buccione. 2004. The role of dynamin in the assembly and function of podosomes and invadopodia. *Front. Biosci.* 9:1944–1953. https://doi.org/10.2741/1348

Morlot, S., V. Galli, M. Klein, N. Chiaruttini, J. Manzi, F. Humbert, L. Dinis, M. Lenz, G. Cappello, and A. Roux. 2012. Membrane shape at the edge of the dynamin helix sets location and duration of the fission reaction. *Cell.* 151:619–629. https://doi.org/10.1016/j.cell.2012.09.017

Murphy, D.A., and S.A. Courtneidge. 2011. The 'ins' and 'outs' of podosomes and invadopodia: characteristics, formation and function. *Nat. Rev. Mol. Cell Biol.* 12:413–426. https://doi.org/10.1038/nrm3141

Ochoa, G.C., V.I. Slepnev, L. Neff, N. Ringstad, K. Takei, L. Daniell, W. Kim, H. Cao, M. McNiven, R. Baron, and P. De Camilli. 2000. A functional link between dynamin and the actin cytoskeleton at podosomes. *J. Cell Biol.* 150:377–389. https://doi.org/10.1083/jcb.150.2.377

Ohniwa, R.L., H. Muchaku, S. Saito, C. Wada, and K. Morikawa. 2013. Atomic force microscopy analysis of the role of major DNA-binding proteins in organization of the nucleoid in Escherichia coli. *PLoS One.* 8:e72954. https://doi.org/10.1371/journal.pone.0072954

Oikawa, T., T. Itoh, and T. Takenawa. 2008. Sequential signals toward podosome formation in NIH-src cells. *J. Cell Biol.* 182:157–169. https://doi.org/10.1083/jcb.200801042

Oikawa, T., M. Oyama, H. Kozuka-Hata, S. Uehara, N. Udagawa, H. Saya, and K. Matsuo. 2012. Tks5-dependent formation of circumferential podosomes/invadopodia mediates cell-cell fusion. *J. Cell Biol.* 197:553–568. https://doi.org/10.1083/jcb.201111116

Oren-Suissa, M., and B. Podbilewicz. 2007. Cell fusion during development. *Trends Cell Biol.* 17:537–546. https://doi.org/10.1016/j.tcb.2007.09.004

Owen, D.J., P. Wigge, Y. Vallis, J.D.A. Moore, P.R. Evans, and H.T. McMahon. 1998. Crystal structure of the amphiphysin-2 SH3 domain and its role in the prevention of dynamin ring formation. *EMBO J.* 17:5273–5285. https://doi.org/10.1093/emboj/17.18.5273

Pan, Y.R., C.L. Chen, and H.C. Chen. 2011. FAK is required for the assembly of podosome rosettes. *J. Cell Biol.* 195:113–129. https://doi.org/10.1083/jcb.201103016

Reubold, T.F., K. Faelber, N. Plattner, Y. Posor, K. Ketel, U. Curth, J. Schlegel, R. Anand, D.J. Manstein, F. Noé, et al. 2015. Crystal structure of the dynamin tetramer. *Nature.* 525:404–408. https://doi.org/10.1038/nature14880

Richardson, B.E., S.J. Nowak, and M.K. Baylies. 2008. Myoblast fusion in fly and vertebrates: new genes, new processes and new perspectives. *Traffic.* 9:1050–1059. https://doi.org/10.1111/j.1600-0854.2008.00756.x

Rodal, A.A., S.J. Del Signore, and A.C. Martin. 2015. Drosophila comes of age as a model system for understanding the function of cytoskeletal proteins in cells, tissues, and organisms. *Cytoskeleton (Hoboken).* 72:207–224. https://doi.org/10.1002/cm.21228

Saini, P., and S.A. Courtneidge. 2018. Tks adaptor proteins at a glance. *J. Cell Sci.* 131:jcs203661. https://doi.org/10.1242/jcs.203661

Schachtner, H., S.D. Calaminus, S.G. Thomas, and L.M. Machesky. 2013. Podosomes in adhesion, migration, mechanosensing and matrix remodeling. *Cytoskeleton (Hoboken).* 70:572–589. https://doi.org/10.1002/cm.21119

Schmid, S.L., and V.A. Frolov. 2011. Dynamin: functional design of a membrane fission catalyst. *Annu. Rev. Cell Dev. Biol.* 27:79–105. https://doi.org/10.1146/annurev-cellbio-100109-104016

Seals, D.F., E.F. Azucena Jr., I. Pass, L. Tesfay, R. Gordon, M. Woodrow, J.H. Resau, and S.A. Courtneidge. 2005. The adaptor protein Tks5/Fish is required for podosome formation and function, and for the protease-driven invasion of cancer cells. *Cancer Cell.* 7:155–165. https://doi.org/10.1016/j.ccr.2005.01.006

Sens, K.L., S. Zhang, P. Jin, R. Duan, G. Zhang, F. Luo, L. Parachini, and E.H. Chen. 2010. An invasive podosome-like structure promotes fusion pore formation during myoblast fusion. *J. Cell Biol.* 191:1013–1027. https://doi.org/10.1083/jcb.201006006

Sever, S., J. Chang, and C. Gu. 2013. Dynamin rings: not just for fission. *Traffic.* 14:1194–1199. https://doi.org/10.1111/tra.12116

Sharma, V.P., R. Eddy, M. Kai, F. Gertler, and J. Condeelis. 2012. Tks5 regulates invadopodium precursor stability through PI(3,4)P-2 in breast cancer cells. *Mol. Biol. Cell.* • • •:23.

Sharma, V.P., R. Eddy, D. Entenberg, M. Kai, F.B. Gertler, and J. Condeelis. 2013. Tks5 and SHIP2 regulate invadopodium maturation, but not initiation, in breast carcinoma cells. *Curr. Biol.* 23:2079–2089. https://doi.org/10.1016/j.cub.2013.08.044

Shen, Y., Z. Wen, Y. Li, E.L. Matteson, J. Hong, J.J. Goronzy, and C.M. Weyand. 2017. Metabolic control of the scaffold protein TKS5 in tissue-invasive, proinflammatory T cells. *Nat. Immunol.* 18:1025–1034.

Shilagardi, K., S. Li, F. Luo, F. Marikar, R. Duan, P. Jin, J.H. Kim, K. Murnen, and E.H. Chen. 2013. Actin-propelled invasive membrane protrusions promote fusogenic protein engagement during cell-cell fusion. *Science.* 340:359–363. https://doi.org/10.1126/science.1234781

Shin, N.Y., H. Choi, L. Neff, Y. Wu, H. Saito, S.M. Ferguson, P. De Camilli, and R. Baron. 2014. Dynamin and endocytosis are required for the fusion of osteoclasts and myoblasts. *J. Cell Biol.* 207:73–89. https://doi.org/10.1083/jcb.201401137

Soulet, F., D. Yarar, M. Leonard, and S.L. Schmid. 2005. SNX9 regulates dynamin assembly and is required for efficient clathrin-mediated endocytosis. *Mol. Biol. Cell.* 16:2058–2067. https://doi.org/10.1091/mbc.e04-11-1016

Srinivas, B.P., J. Woo, W.Y. Leong, and S. Roy. 2007. A conserved molecular pathway mediates myoblast fusion in insects and vertebrates. *Nat. Genet.* 39:781–786. https://doi.org/10.1038/ng2055

Stowell, M.H., B. Marks, P. Wigge, and H.T. McMahon. 1999. Nucleotide-dependent conformational changes in dynamin: evidence for a mechanochemical molecular spring. *Nat. Cell Biol.* 1:27–32. https://doi.org/10.1038/8997

Sweers, K., K. van der Werf, M. Bennink, and V. Subramaniam. 2011. Nanomechanical properties of α-synuclein amyloid fibrils: a comparative study by nanoindentation, harmonic force microscopy, and Peakforce QNM. *Nanoscale Res. Lett.* 6:270. https://doi.org/10.1186/1556-276X-6-270

Thompson, O., I. Kleino, L. Crimaldi, M. Gimona, K. Saksela, and S.J. Winder. 2008. Dystroglycan, Tks5 and Src mediated assembly of podosomes in myoblasts. *PLoS One.* 3:e3638. https://doi.org/10.1371/journal.pone.0003638

Vasyutina, E., B. Martarelli, C. Brakebusch, H. Wende, and C. Birchmeier. 2009. The small G-proteins Rac1 and Cdc42 are essential for myoblast fusion in the mouse. *Proc. Natl. Acad. Sci. USA.* 106:8935–8940. https://doi.org/10.1073/pnas.0902501106

Warnock, D.E., J.E. Hinshaw, and S.L. Schmid. 1996. Dynamin self-assembly stimulates its GTPase activity. *J. Biol. Chem.* 271:22310–22314. https://doi.org/10.1074/jbc.271.37.22310

Yu, C.H., N.B. Rafiq, A. Krishnasamy, K.L. Hartman, G.E. Jones, A.D. Bershadsky, and M.P. Sheetz. 2013. Integrin-matrix clusters form podosome-like adhesions in the absence of traction forces. *Cell Reports.* 5:1456–1468. https://doi.org/10.1016/j.celrep.2013.10.040